LINC

Learning about Interacting Networks in Climate

Marie Curie Initial Training Networks (ITN)

FP7- PEOPLE - 2011- ITN

Grant Agreement No. 289447

WorkPackage WP4: *Future Climate Change*

Deliverable D4.3

Report on the identification of processes associated with climate shifts in the S.H.

Marcelo Barreiro, Universidad de la República, Uruguay

Release date: 30 Octubre 2014

Status: *public*

EXECUTIVE SUMMARY

One of the main objectives of the WP4 is to determine regime shifts in the evolution of the 20th century climate by analyzing reanalysis data and model simulations. In the Deliverable D4.2 we have reported about our advances in understanding the influence of the global tropical oceans on precipitation over Southeastern South America during spring time. The main finding was that this influence shows interdecadal variability and that different oceans play the most important role at different times of the 20th century, even though the equatorial Pacific dominates. As a way to understand the causes of the observed variability in the role of the tropical oceans we studied the evolution of the global atmospheric connectivity at upper levels during the 20th century centering the analysis on the 200 hPa eddy geopotential field. This field is particularly important for the transmission of the influence from the tropics toward the extratropics in the form of Rossby wave teleconnection patterns.

For this purpose we build networks from two different reanalysis data sets by using both linear and nonlinear statistical similarity measures to determine the existence of links between different regions of the world in the two halves of the last century. We further use symbolic analysis to emphasize intraseasonal, intraannual and interannual time scales. Both linear and nonlinear networks have similar structure and evolution, showing that the most connected regions are on the tropics over the Pacific ocean and that the southern hemisphere extratropics have more connectivity in the first half of the 20th century.

Changes over the Pacific main connectivity regions are analyzed in more detail. All the different networks, except for the intraseasonal time scales, show similar behavior with a decreasing connectivity from the early 1900 up to 1940-1956, when it starts to increase until the present. The intraseasonal network in western Pacific has a unique behavior with an increasing trend in almost all the century. In central Pacific, on the other hand, all the networks, including the intraseasonal, show a minimum of connectivity in 1940-1950.

In order to separate the internal and forced connectivity networks and study their evolution through time, an ensemble of atmospheric general circulation model outputs is used. The results suggest that the main connectivity pattern captured in the reanalysis networks are due to the oceanically-forced component, particularly on interannual time scales. Moreover, the atmospheric internal variability seems to play an important role in determining the intraseasonal time scale networks.

Deliverable Identification Sheet

Grant Agreement No.	**PITN-GA-2011-289447**
Acronym	**LINC**
Full title	**Learning about Interacting Networks in Climate**
Project URL	http://climatelinc.eu/
EU Project Officer	Lucia PACILLO

Deliverable	**D4.3 Report on the identification of processes associated with climate shifts in the S.H.**
Work package	**WP4 Future Climate Change**

Date of delivery	**Contractual**	M 30	**Actual**	30-Oct-2014
Status	version. 1.00		final ☑	draft
Nature	Prototype	Report ☑	Dissemination	
Dissemination Level	Public	Consortium ☑		

Authors (Partner)	**Marcelo Barreiro, Universidad de la Republica, Uruguay**			
Responsible Author	Marcelo Barreiro		**Email**	barreiro@fisica.edu.uy
	Partner	Universidad de la República	**Phone**	

Abstract (for dissemination)	Report on the Deliverable 4.3 of WP4 of the LINC project.	
Keywords	Teleconnections, connectivity, climate evolution.	

TABLE OF CONTENTS

EXECUTIVE SUMMARY.....II
TABLE OF CONTENTS.....IV
1 INTRODUCTION.....1
2 DATA 2
3 RESULTS.....6
4 SUMMARY 19
5 REFERENCES 20

1 INTRODUCTION

In the last 15 years, since the pioneering works on complex networks (Watts and Strogatz, 1998; Barab´asi and Albert, 1999), the use of this statistical methodology of analysis has allowed significant advances in a broad variety of scientific disciplines including social systems, internet, neural networks, metabolic networks, gene expresions among many others (Albert and Barabasi, 2002; Newman, 2010).

The study of the climate system has been also benefited from the application of this new theoretical framework and several manuscripts have been written in the past years (Tsonis et al., 2004, 2006; Donges et al., 2009; Gozolchiani et al., 2008; Barreiro et al., 2011) providing valuables insights into climate dynamics. As it is well known, the climate system is characterized by phenomena with many different temporal and spatial scales, so that a variety of network approaches have been proposed to study different modes of variability. For example, a large number of articles have been dedicated to the analysis of El Nino-Southern Oscillation phenomenon (Tsonis et al., 2008; Gozolchiani et al., 2008; Martin et al., 2013; Radebach, 2013) and how it affects the connectivity of the network (see also Deza et al. in this volume).

El Nino has been shown to influence the climate of far away regions through the excitation of tropical atmospheric anomalies that propagate longitudinaly within the tropics andmeridionally to the extratropical regions. The theory that tries to explain this remote connections, or teleconnections, is mainly based on linear wave dispersion of Kelvin and Rossby waves (Held, 1983; James, 1994). Even though there have been several attempts to improve this description including the influence of El Nino through other mechanisms (Seager et al., 2003) the understanding of atmospheric teleconnections is not yet complete.

Here we aim to deepen the understanding of atmospheric teleconnections analyzing the 200 mb eddy geopotential heigth field from a complex network perspective. This levelis chosen because it is the height of maximum tropical divergence which is crucial for the excitation and propagation of tropical and extratropical anomalies like Rossby waves trains (Trenberth et al., 1998). A second objective of this study is to analyze potential changes in the atmospheric connections during the last century. We focus on the connectivity of tropical Pacific because it has been shown to be the globally most connected region by several studies (Donges et al., 2009; Barreiro et al., 2011).

In order to accomplish these objectives we analyze two atmospheric reanalysis data sets, which represent the best estimates available of the historical atmospheric evolution (Broennimann et al., 2009), and an ensemble of experiments performed with an Atmospheric General Circulation Model (AGCM). The networks determining the connectivity among nodes are built in terms of the statistical similarity of the corresponding time series. We use both linear and nonlinear statistical measures (Donges et al., 2009; Barreiro et al., 2011): the linear Pearson correlation (PC) and the nonlinear mutual information (MI). Alternatively, as the PC and the MI, obtained from on histogram-based probability density functions (PDFs), do not take into account the temporal order of the time series, we introduce the ordinal patterns methodology proposed by (Bandt and Pompe, 2002) (BP). This method allows us to consider different time scales with the MI as in Barreiro et al. (2011). In general, the networks are represented graphically as two-dimensional maps by plotting the area weighted connectivity AWC, which represent the fraction of the total area of the Earth to which each 100 node is connected.

The total atmospheric variability can be decomposed in a component due to the intrinsic dynamics of the atmosphere that would occur even in the absence of changes of the boundary conditions, and another component due to the forcing of the surface ocean conditions. The latter is potentially more predictable as it depends on the evolution of the sea surface temperature, which varies on much longer time scales than the atmospheric fields. In some regions, like the tropical Pacific, the ocean-atmosphere interaction allows the prediction of sea surface temperature anomalies (i.e. the development of El Nino) with up to 6-9 months in advance (Neelin et al., 1998). Thus, it is extremely important for seasonal climate prediction to be able to separate and determine the dynamics that characterizes the intrinsic and forced atmospheric variability. In this study we use the AGCM output to determine if the observed 20th century changes in connectivity are related to the forced or intrinsic dynamics.

Our results show that the most connected regions are in the tropical Pacific and the overall network structure is broadly similar using both the linear and nonlinear statistical measures when no time scales are considered. However, using the BP methodology, the nonlinear symbolic analysis reveals several structural changes in the networks. Some regions become more relevant depending on the time scale considered, such as the southern hemisphere, relatively more important on the intraseasonal time scales, or the northern Pacific, more relevant on the intraannual time scales. Moreover, the changes on the main connectivity regions are analyzed and different behaviors are observed for the intraseasonal time scale networks, where the western Pacific increases its connectivity along all the period considered

while the other networks present similar evolution, decreasing their connectivities in the mid-century. This article is organized as follows: Section II provides a description of the data analyzed, model used and a summary of the methodology employed. Section III presents the results, and finally in Section IV we present a summary and discuss the main results.

2 DATA AND METHODOLOGY

2.1 Data

We use monthly average geopotential height at 200 mb from the NOAA 20th Century Reanalysis (Compo et al., 2011) and from the NCEP CDAS1 reanalysis data (Kalnay et al., 1996). It is important to have in mind that a reanalysis is constructed blending observations in an AGCM, and thus the value of the reanalysis compared to a simple model run increases where there are enough observations to constraint the model solution. Previous to 1950 observations were very limited globally and thus the reanalysis may not represent as much reality as it does represent the model solution. In the southern hemisphere the situation is even more difficult because there were very few observations previous to the satellite era that began in 1979. Given these limitations the results of this study must be considered as a first approximation of reality based on the best information available to date about the evolution of the 20th century atmospheric circulation.

In addition, we consider the ouput of the Atmospheric General Circulation Model from the International Center for Theoretical Physics (ICTP-AGCM) forced with global historical sea surface temperature (ERSSTv.2, Smith and Reynolds (2004)). The ICTP-AGCM is a full AGCM with simplified physics and an horizontal resolution of T30 with 8 vertical levels (Molteni, 2003; Kucharski et al., 2006). The performance of the ICTP-AGCM in representing the large scale atmospheric dynamics is comparable to

that of state of-the-art AGCMs and has been used to study global climate variability, including the influence of the oceans on the circulation (Barreiro et al., 2008; Barreiro, 2009; Kucharski et al., 2008, 2009). Reanalysis and model output are distributed in regular latitute-longitude grids with every point characterized by a time series of the variable of interest. The characteristics of each data set are summarized in table 1. The geopotential height at 200 mb has a meridional structure dominated by relatively large values in the tropical regions decreasing toward the poles. To highlight connections that are deviations from this zonal structure we consider the eddy geopotential height which is calculated removing the zonal mean of each latitudinal band for every month.We further consider monthly anomalies, that is, the mean annual cycle is removed previous to analysis, and the time series are linearly detrended at each grid point.

Source	Resolution	Time period	Dimensions	
NCEP CDAS1	2.5^o	$[1949, 2011]$	$N = 10224$	$T = 756$
NOAA 20th Cent	2^o	$[1901, 2009]$	$N = 16020$	$T = 1308$
ICTP AGCM	3.75^o	$[1901, 2006]$	$N = 4980$	$T = 1272$
EN34 index	–	$[1901, 2006]$	$N = 1$	$T = 1308$

Table 1 – Characteristics of data, N: number of grid points, T: number of months.

2.2 Network Building

To build the network every pair of points over the grid is linked whenever a significant statistical similarity between the correspondent time series is detected. Let x(t) ={x_i(t)} i=1...N with t = 1...T be the 200 mb eddy geopotential height anomaly field and S(xi,xj) = Sij the similarity measure between the nodes i and j. Then the elements of the climate network adjacency matrix A are:

$A_{ij} = \Theta(|S_{ij}| - \tau) - \delta_{ij}$;

where Θ() is the Heaviside step function, δ is the Kronecker delta and τ is a statistical threshold introduced to avoid spurious connections. In order to set the threshold value we use the same criterium for every network, randomnly relabeling the elements within each time series such that the distributions remain unchanged, and taking a fixed quantile value (99%) of the statistical similarity measure of every possible combination as a threshold. Thus, the null hypothesis of independence can be rejected if the statistical similarity value of the original time series is above this threshold at a 0.01 level of significance. Recently, (Palus et al., 2011) have shown that two time series that have some autocorrelation, or persistence (defined as the lag time when the autocorrelation drops below 1/e), induce a bias in the connectivity measure. To avoid this supposed bias (Palus et al., 2011) suggest considering the persistence of the time series when calculating the connectivity threshold, and show that the network topology differs significantly when this is taken into account. In climate data the persistence at a particular location is due to local and remote processes. The part of the persistence due to local processes is the one that should be considered in the connectivity threshold because it introduces a bias in the connectivity. However, the persistence due to remote processes is a real connection that occurs through atmospheric circulation anomalies and should be considered when calculating connectivity measures as the area weighted connectivity used here (see below).

The persistence of the 200 mb eddy geopotential height of the NOAA 20th Cent reanalysis data is shown in the left panel of Fig. 1, where it can be seen that the persistence is one month for the extratropics and from 2 to 6 months in the tropical band with maximum in the Pacific. This result emphasizes the large internal atmospheric variability present inthe extratropics and the dominant role of the oceans forcing in the tropical band. The right panel of Fig. 1 shows the persistence after the effect of El Nino (El Nino 3.4 index) has been linearly removed by a regression procedure. Clearly,most of the persistence in the tropical band is due to the El Nino phenomenon that is known to affect the global tropics through the propagation of Kelvin waves (e.g. Lintner and Chiang, 2007). Given that El Nino persists for about 6 months, the connections from the tropical Pacific to the rest of the tropics is also maintained. After El Nino is removed the persistence in the tropics is about 2 months, which might be because the linear procedure was not enough to remove the El Nino influence completely or due to the existence of local processes that slightly enhance persistence. Nevertheless, it is clear that a persistence of 1 month is characteristic of most of the world and thus randomnly mixing the time series on individual points of the grid provides a good test for the connectivity. This procedure assures to recognize the importance of the tropical Pacific in the global connectivity as clearly seen in Fig. 2.

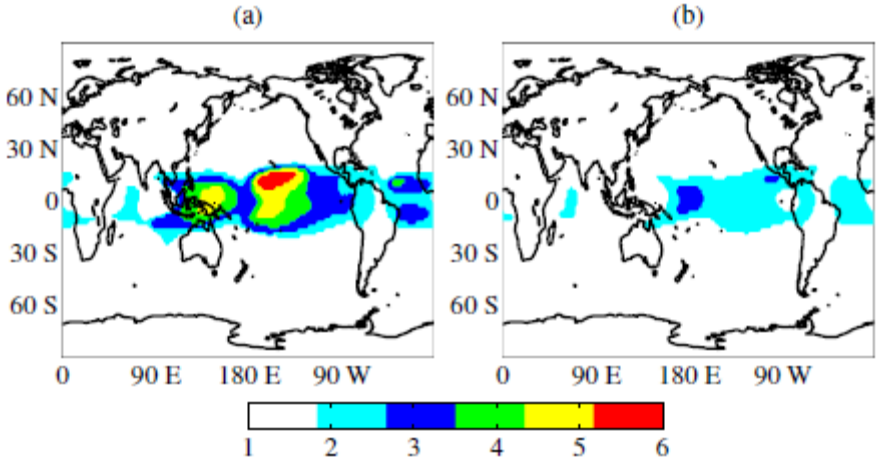

Figure 1 - Persistence of the 200 mb eddy geopotential height field of the 20th Century Reanalysis data from NOAA with (a) and without (b) the EN34 component.

We constructed networks using linear and nonlinear measures of connectivity. Networks made of purely linear interaction are constructed evaluating the statistical interdependency between the nodes with the Pearson correlation. Nonlinear connectivity is evaluated using a quantity from information theory, the mutual information:

$$M_{ij} = \sum_{m,n} p_{ij}(m,n) \log \frac{p_{ij}(m,n)}{p_i(m)\, p_j(n)}$$

where pi and pj are the marginal probability density functions of xi and xj respectively, and pij the joint probability density function. According to information theory, mutual information is a measure of how much information about xi is gained by knowing xj . It is easy to see that if the time series are independent, pij(m,n) = pi(m)pj(n), therefore Mij = 0. It is important to notice that both mutual information and linear correlation are

symmetric quantities. The usual way of obtaining the PDF of a time series is by building traditional histograms. Generally, the numbers of bins in the histogram are chosen according to the time series length in order to have good statistics. One important characteristic about using histograms is that the time-related information is only considered in the joint probability because when using histograms for representing the marginal probabilities all the temporal information is neglected and, as with linear correlation, there is no emphasis on any particular time scale.

To overcome this limitation, Bandt and Pompe (BP) methodology (Bandt and Pompe, 2002) based on symbolic analysis is employed to separate different time scales. This symbolic analysis consists of building the PDFs by analyzing the patterns formed by consecutive values in the time series. Specifically, each time series xi(t) is divided into T-D overlapping D-dimensional vectors. These vectors are represented as ordinary patterns (OP), in the sense that each element is replaced by a number from 0 to D-1 depending on its ordinal position (i.e. 0 for the lowest and D-1 for the largest). Then, each vector is assigned one of the D! possible configurations. For instance, if D = 3 the possible configurations are (012 021 102 120 201 210), and, for example, the sequence (2.3;0.7;8.7) corresponds to the 102 pattern. The BP methodology needs only a weak stationary assumption that the probability for $x_i^t < x_i^{t+D}$ should not depend on t. This is satisfied removing the linear trend in the data. Another condition to calculate the PDFs adequatelly is that T >> D! i.e. the number of vectors must be much larger than the numbers of possible OPs.

There is an embedding dimension given by the D parameter of the BP method that fixes the causality time scale. This is the main difference with classical histogram-based technique used to build the probability density functions. An important advantage is that it is possible to build sequences of patterns not only with consecutive values but with an arbitrary time interval t between them. In this study we have chosen to work with D = 3 and t = 1,4 and 12 months intervals to characterize atmospheric processes on intraseasonal, intraannual and interannual time scales, respectively.

2.3 Area Weighted Connectivity

The network representation of a climate field helps to obtain valuable insight into the climate dynamics, however, it is clear that the specific procedure to build the network is decisive on the information it provides. Moreover, once the network is built there are different analysis that can be done in order to deepen our understanding of the dynamics that is being analyzed, as calculating the betweennes centrality for each node (Donges et al., 2009) or detecting the communities underlying in the system (Tsonis et al., 2011).

Following the procedure proposed in previous studies on climate networks (Tsonis et al., 2006; Donges et al., 2009; Barreiro et al., 2011), to analyze the changes in the atmospheric connectivity in the 20th century, we use the area weighted connectivity (AWC) function. The AWC provides the fraction of Earth that each node is connected to, similar to the k-degree usual in complex networks but area weighted and normalized to be within 0 and 1.

This study is concerned with analyzing the changes in the atmospheric connectivity during the last hundred years which, as will be shown below, is dominated by the tropical Pacific. Thus, to further understand the changes in these regions we calculate the evolution of the AWC in two boxes in the central and western Pacific using the

NOAA 20th century reanalysis data. Specifically we considered the nodes in the following regions:

– Western Pacific (WP): [3ºS-7ºS;129ºE-135ºE]

– Central Pacific (CP): [3ºS-7ºS;151ºW-157ºW].

The evolution is measured taking 30-year sliding windows in steps of one year and calculating the average AWC for each region.

2.4 Intrinsic and forced atmospheric variability

To aid the interpretation of the networks obtained with reanalysis data we consider the output of the ICTP-AGCM. In particular, as explained in the introduction we are interested in separating the networks associated with intrinsic (or internal) atmospheric variability and with oceanically-forced atmospheric variability. So, we constructed an ensemble of 9 ICTP-AGCM runs where the model is forced with global historical sea surface temperatures as boundary conditions and slightly different atmospheric initial conditions. Given the chaoticity of the atmospheric dynamics this setup generates n = 9 equiprobable realizations of the atmospheric evolution. The procedure to separate internal from forced atmospheric variability is done in two steps: we fist estimate the focred component of the variability as the common signal in all ensemble members by taking the ensemble average. Secondly, to estimate the internal variability we remove the forced component from each ensemble member. To characterize the newtowrk atmospheric internal variability we calculated the AWC for every ensemble member and then averaged the individual AWCs.

2.5 Principal component analysis

To further aid in the role of the tropical Pacific setting the connections, we removed its contribution and constructed again the AWC maps. To do so we built the AWC maps after linearly removing the two first leading Empirical Orthogonal Functions (EOFs) calculated for the tropical Pacific. The difference between the AWC maps after these EOFs are removed allows to associate regions of large connectivity with known modes of variability. We calculated the EOFs of the NOAA 20th century reanalysis data in the region [90E-70W;30N-30S] and considered the two eigenvectors with largest eigenvalues of the covariance matrix, which together explain about a quarter of the total variance.

3 RESULTS

3.1 Area Weighted Connectivity maps

Being our goal to analyze changes in the structure of atmospheric connectivity on different time scales since the beginning of the 20th century, we divide the NOAA 20th century reanalysis data into two equal length halves: [January 1901 - December 1955] and [January 1955 - December 2009]. The resulting networks built with Pearson correlation (PC) and mutual information with the probability density functions based on classical histograms (MIH) are represented by the AWC function in Fig. 2.

The spatial structure of the maps obtained with the different measures of connectivity is globally very similar. The main difference lies in the number of connections, that represent the quantity of significant links, which is bigger in the PC networks than in the MIH networks. The links density δ

$$\delta = \frac{\sum_{ij}^{N} A_{ij}}{N(N-1)}$$

is defined to quantify this property. The networks constructed with PC present δ~0.30 while the corresponding value with MIH is δ~0.20.

In all the cases, the most connected areas are located in the tropics, particularly in the central Pacific and to a lesser extent over the Atlantic ocean, south Asia and over Indonesia between the Indian ocean and western Pacific. This larger connectivity in the tropics with both methodologies agrees with our current understanding of tropical dynamics. Likewise, but with lower strength in the sense that they vanish for lower threshold values than the tropics, there are some extratropical regions that are relevant for their number of connections, such as south and north Pacific which reflect the teleconnection patterns in both hemispheres through the propagation of Rossby waves.

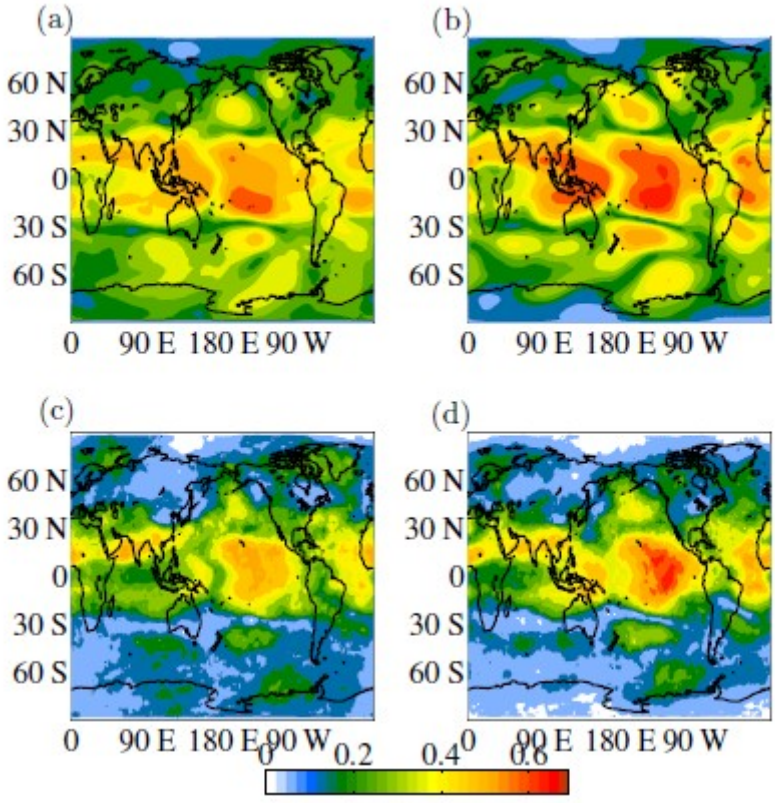

Figure 2 – AWC connectivity map of the 200 mb eddy geopotential height field with the graph construction methodology applied to the 20th Century Reanalysis data from NOAA. Statistical similarity measures and period taken: (a) PC (1901-1955), (b) PC (1955-2009), (c) MI with classical histograms (1901-1955), and (d) MI with classical histograms (1955-2009).

The area of largest connectivity in the central Pacific shows differences according to the methodology: while using PC the area of maximum connectivity is to the south of the equator at about 170W-130W, using MIH the (less well defined) maximum is centered on the equator further to the east.

Some additional observations can be made from Fig. 2. Firstly, we note that there are more significant links in the southern hemisphere than in the northern hemisphere, especially in the first period. A structure, displaying the signature of Rossby waves propagating from the tropics through the southern Pacific to the south American continent, can be distinguished in all the panels. It is also interesting to look at the connectivity spot located in the western Pacific and south Asia which increases its connectivity in the second period. The opposite occurs in the region west of India and the southern Indian ocean west of 90E which decreases its connectivity, specially with the MIH. These variations suggest that the Indian ocean excites the Rossby wave train that propagates from the Indian ocean sector toward the south Pacific with more strength in the period 1901-1955.

3.2 Ordinal pattern analysis

Figure 3 presents the results of the AWC calculated with the BP methodology for intraseasonal, intraannual and interannual time scales using D=3 as the embedding dimension. Irrespective of the period considered, the tropics always dominate the connectivity on all time scales. However, the connectivity of the tropical region increases with the time scale, while that of the extratropics does not vary to the same extent. In fact, connectivity in the northern extratropics is largest on intraannual time scales (particularly in the northern Pacific), while in the southern extratropics is fairly constant except in the southern subtropical Pacific within [30S-40S,160W-120W] where connectivity increases substantially on interannual time scales. The relative maximum in this region in the AWC maps is not as well defined in the intraseasonal and intraannual networks as in the interannual networks, but does appear in the AWC maps calculated with PC and MIH in Fig. 2. This suggests that the symbolic analysis is succesful in separating processes according to their time scales. Regarding links density, $\delta \sim 0.14$ for intraseasonal networks and $\delta \sim 0.16$ for intraannual and interannual networks.

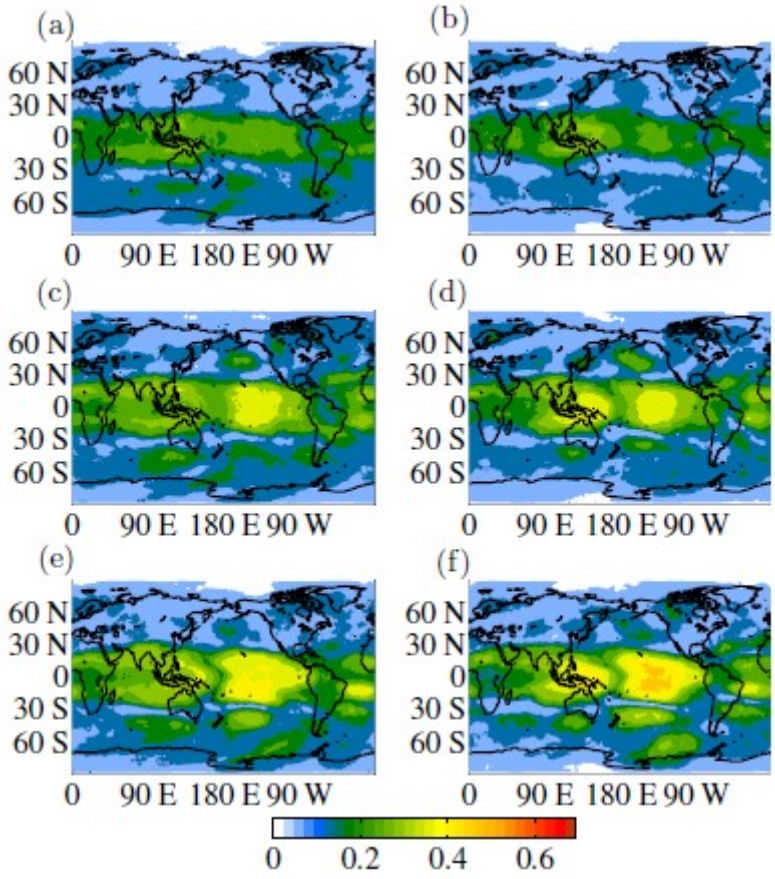

Figure 3 – AWC maps of the 200 mb eddy geopotential height field obtained from the MI using the BP symbolic analysis for different time scales: intraseasonal (Δt = 1) (1901-1955) (a) and (1955- 2009) (b); intraannual (Δt = 4) (1901-1955) (c) and (1955-2009) (d), and interannual (Δt = 12) (1901-1955) (e) and (1955-2009) (f).

The changes in AWC between the two time periods considered in Fig. 2 are further explored in Fig. 3. On intraseasonal time scales, Δt=1 month, the area of larger connectivity in the first period is over the tropical Pacific and between south Asia and north Oceania, while in the second half the global maximum is in the western Pacific and the central Pacific region is less connected. Also, the first period shows larger connectivity areas in the southern Indian ocean and southern extratropics with similar differences in structure between the two periods as with PC and MIH (Fig. 2). This behavior is also valid for longer time scales.

In the case of intraannual time scales, Δt=4 months, there are more links in the northern hemisphere, particularly over oceanic areas and there are also some differences in the connectivity of the tropical Pacific in both time periods, while in the eastern sector during the second period there is lower intensity, the opposite occurs in the western region, such as with intraseasonal networks. On the other hand, both central and western Pacific are more connected during the second half of the 20th century than during the first half on interannual time scales, Δt=12 months.

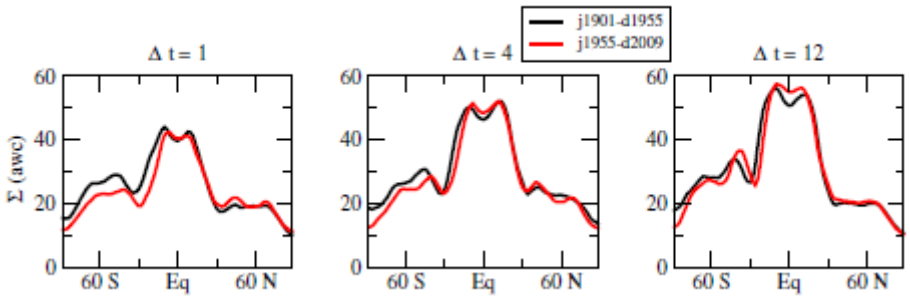

Figure 4 - Meridional sum of the AWC for the NOAA networks built by using the BP methodology with $\Delta t=1$, $\Delta t=4$, $\Delta t=12$ for both time periods (black: 1901-1955; red: 1955-2009).

This different behavior in the evolution of the connectivity in certain regions depending on the time scale can also be noticed over Canada, with larger connectivity in the first period in the intraannual networks, while in the interannual is the other way around. Intraannual and intraseasonal networks show also an increament in the connectivity off the coast of south Brazil, contrary to what is seen in PC and MIH networks in Fig. 2. These facts suggest different evolutions of atmospheric processes on different time scales during the period of study.

The hemispheric asymmetries in the AWC are quantified in Fig. 4, where the longitudinal sum of AWC versus latitude is plotted. All the curves present a local minimum on the equator and two similar maxima near 10S and 10N. Also, on intraannual time scales the tropics are more connected during the first period, while on intraseasonal and interannual the opposite is true. Finally, the plots also show that the relatively larger connectivity seen in the southern hemisphere during period 1901-1955 is maximum on intraseasonal time scales and decreases on longer time scales.

In order to test the robustness of the results we have also constructed the AWC using the 200 mb eddy geopotential height of the NCEP CDAS1 reanalysis during the same time period as the second half of the NOAA data. Figure 5 shows the AWC maps derived from the Pearson correlation and the mutual information with the symbolic analysis. The values of δ obtained are in good agreement with the maps showed in Figs. 2 and 3. The maps recover the same characteristics obtained for the NOAA 20th century reanalysis, for example, relatively larger connectivity in the northern Pacific on intraannual time scales, a weakly connected central Pacific on intraseasonal times scales and a strongly connected south Pacific on interannual time scales. Moreover, there is a weaker indication of a wave train from the Indian ocean on any time scales.

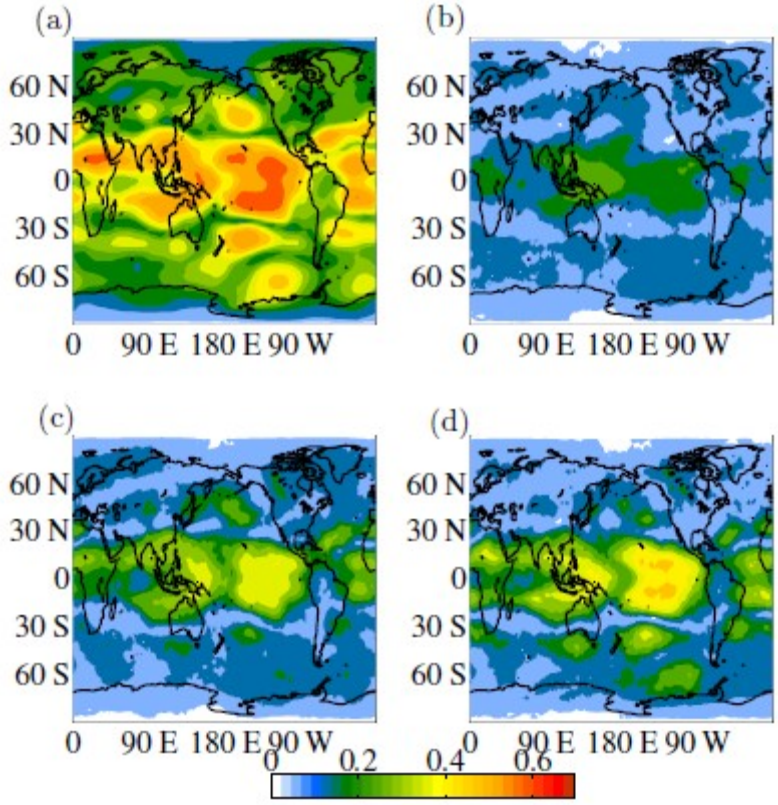

Figure 5 - AWC maps obtained from NCEP/NCAR reanalysis data. The statistical similarity measures used: PC (a), MI with the BP methodology: Δt=1 (b), Δt=4 (c) and Δt=12 (d).

3.3 Temporal evolution of the AWC

We study further the time evolution of the connectivity for the western Pacific (WP) and central Pacific (CP) regions, defined above. To enhance statistics, especially with the mutual information calculated with symbolic analysis, we took 30-year windows such that T=360 months.

Fig. 6 and Fig. 7 show plots of AWC versus time for all the different networks for the WP and CP zones respectively. The behavior of the AWC for both regions depend on the methodology used. Basically the overall evolution in the PC, MIH and interannual networks is very similar but intraannual and intraseasonal networks behave differently. In western Pacific, Fig. 6, the mean connectivity of the WP box presents a general decrease for the PC, MIH and intraseasonal networks from the beginning of the century up to approximately 1940, when the connectivity starts an increasing trend until the end of the century. The connectivity of the intraannual network behave quite constant during the first decades, and from 1956 onwards it starts increasing up to the end of the record. On the other hand, the AWC of the intraseasonal networks has a small but positive trend during all the period considered.

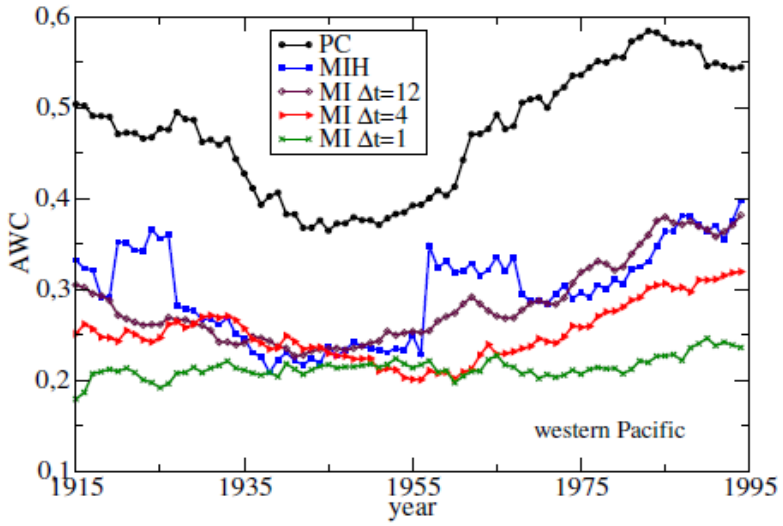

Figure 6 - Temporal evolution of the AWC in the WP box. The networks are built by evaluating 30 year windows of the 200 mb eddy geopotential height field (NOAA) with every methodology used in this work. For each mean AWC value the time period corresponding to 15 years before and 15 years after were considered.

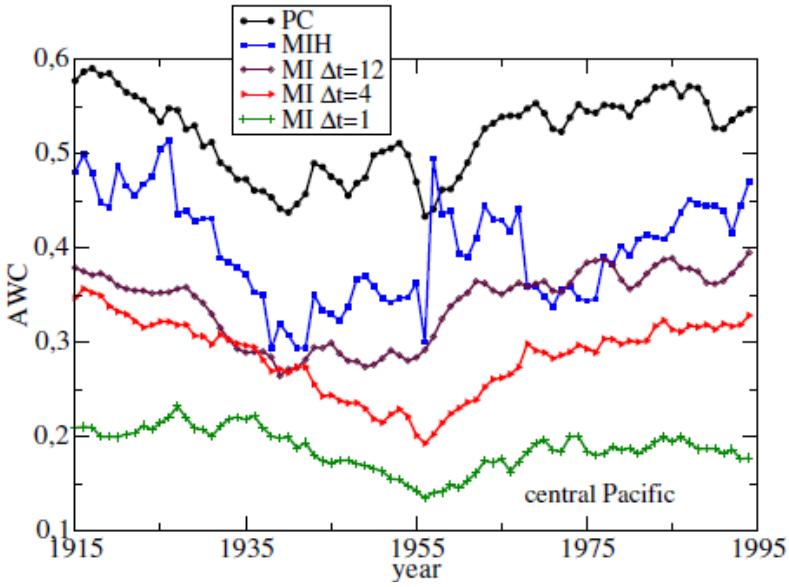

Figure 7 – Same as Figure 6 but for CP box.

PC, MIH and interannual networks show similar behavior in the connectivity of CP box, Fig. 7, starting with a negative trend until 1940 and then an increasing the connectivity to the end. On the other hand, the intraannual and intraseasonal networks maintain the negative trend a few more years, starting the increasing period in 1956 such as the WP box in the intraannual case.

Except in the intraseasonal case, the connectivity values of central Pacific are larger than in western Pacific. It is important to mention that the evolution of the connectivity in the MIH networks presents two periods, 1920-1926 and 1956-1967 of anomaly higher values in both regions analyzed. We further analyzed this fact and observed that

the new connections in both periods are located in the extratropics and with no clear structure, so we assume that might be related to noisy behavior.

Figure 8 shows the statistically significant mean Pearson correlation values of the CP and WP boxes for 1915, 1940 and 1995. In agreement with the time evolution shown in Figs. 6 and 7, it is clearly seen that in the 30 years centered in 1940 the connectivity of these regions is smallest. For the WP it is evident the increase in global connectivity seen in the last decades of the century, particularly due to stronger connections with the tropical Atlantic. These maps also show that the CP and WP are not independent on each other, which is expected because phenomena like El Nino connect both regions through changes in the Walker circulation.

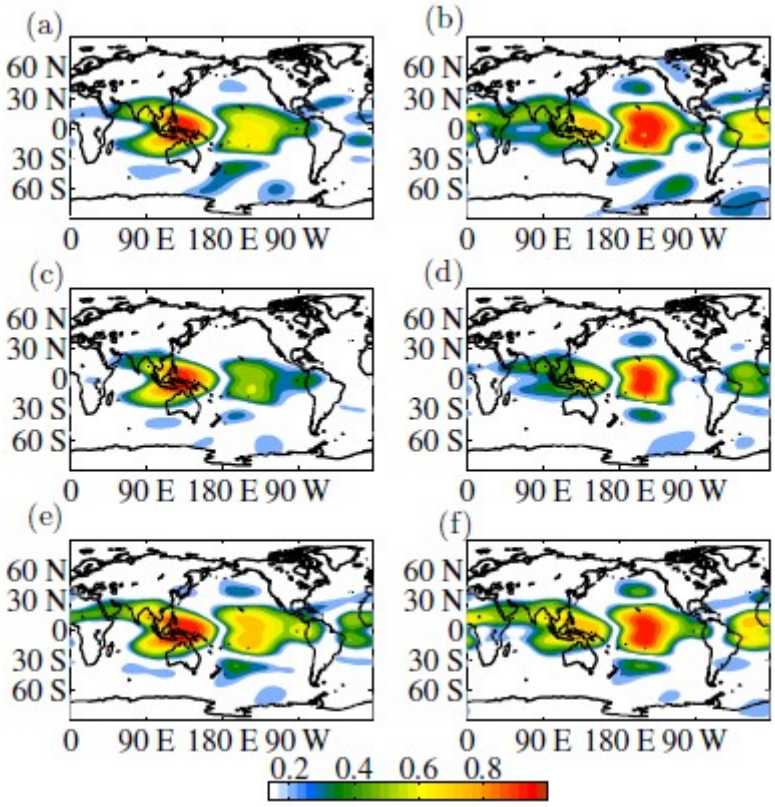

Figure 8 - Maps of the cross-correlation using the NOAA data. The color represents the mean value of the PC of each location with the WP and CP boxes (defined in the text) taking 30-year windows centered at 1915, 1940 and 1995. Panels (a) and (b) correspond to 1915, WP and CP resp. panels (c) and (d) to 1940, WP and CP respectively, and panels (e) and (f) to 1995, WP and CP respectuively.

3.4 Intrinsic and forced variability

Nine ICTP-AGCM model runs with the same sea surface temperature boundary condition and slightly different atmospheric initial conditions were conducted. As it is explained in the methodology section, this allows to separate the AWC function of the forced and internal variability components. In this case, to continue comparing the behaviors in the connectivity of the networks with time, and as the time interval covered by the model output is from 1901 until 2006, the resulting halves are [January 1901, December 1953] and [January 1954, December 2006], with T=636. Even though the

periods do not match exactly with those of the reanalysis, they only differ in two out of 53 years and thus the statistics should be fully comparable.

The forced component AWC maps, obtained by the BP mutual information methodology are shown in Fig. 9. All time scales considered present similar spatial structures for both time periods considered with maxima in the tropics and wavy patterns in the extratropics.

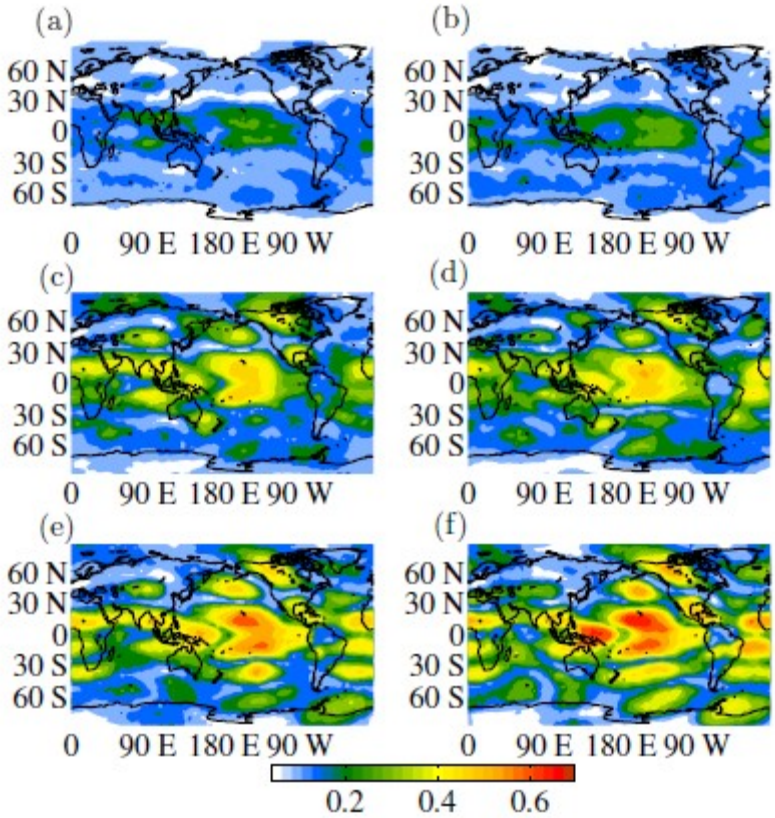

Figure 9 - AWC maps of the ICTP-AGCM oceanically-forced component. The networks are built by evaluating the mutual information with the BP methodology: Δt = 1: (1901-1953) (a) and (1954-2006) (b), Δt = 4: (1901-1953) (c) and (1954-2006) (d), and Δt = 12: (1901-1953) (e) and (1954-2006) (f).

The main difference is the intensity of the connectivity, during the second period the number of connections increases on all the time scales networks. Also, on intrannual time scales northern hemisphere regions are more connected than on intraseasonal time scales and are larger than in the southern hemisphere. On interannual time scales the connectivity is similar in the northern and southern extratropics, and the model recover the highly connected region in the south Pacific located at about [35S,150W].

Comparison with reanalysis reveals very similar structures suggesting that most of the connectivity seen in Fig. 3 are due to oceanically-forced variability. The largest differences occur on intraseasonal time scales in the Indo-Pacific region (particularly in the second half) where the model shows weaker connectivity. Also regarding the reanalysis comparison, it can be noticed that the spatial structure is quite similar except for differences in strength, but there are less changes between the first and second halfs of the 20th century. This might suggest that the reanalysis differences between both time intervals considered are mostly because of the internal variability.

Figure 10 shows the longitudinal sum of AWC versus latitude for different time scales. Comparing with the reanalysis, the curves obtained are less smooth but the general shapes are similar. The values of AWC are, as expected, substantially smaller than in the reanalysis given that internal variability has been filtered. The differences in magnitudes are smaller on longer time scales, indicating the dominant role of the oceans in the interannual global connectivity.

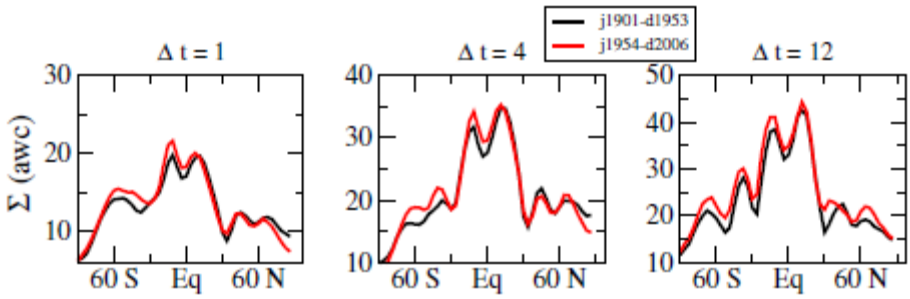

Figure 10 - Meridional sum of the AWC function for the ICTP-AGCM networks built by using the BP methodology with Δt = 1, Δt = 4 and Δt = 12, for both time periods (black: 1901-1953, red: 1954- 2006). It is a measure of how much connections each latitude has.

As in reanalysis data the second period shows enhanced connectivity in the tropics for every time scale. There are asymmetries between the two maxima near the equator that are, however, not present in the reanalysis data networks. Moreover, in the southern hemisphere extratropics the intraseasonal networks show largest connectivity in the second period, opposite to the results obtained in reanalysis. This suggests that atmospheric internal variability plays an important role in the connectivity of the southern extratropics on intraseasonal time scales.

The AWC maps of internal atmospheric variability are shown in Fig. 11. Both Pearson correlation and mutual information with Δt=1 and 4, have mostly the same structure but differ where global maxima are located.

On intraseasonal time scales the regions of maximum connectivity are in the western Pacific and in the southern extratropics. There are clear connections in the southern hemisphere between south Pacific, south America and south Atlantic. There is also a small difference between the two periods: the connectivity in the western Pacific region increases and it decreases in the central Pacific, similarly as with the NOAA 20th century reanalysis data. This result, together with the AWC maps of the forced atmospheric variability suggest that the changes in connectivity observed in the reanalysis during the 20th century are due to changes in both forced and intrinsic components.

On intraannual time scales, on the other hand, the AWC maps present the same well connected spots as the intraseasonal case but also additional regions, mainly in north Pacific and north Atlantic. The wavy patterns suggests the existence of Rossby waves propagation all over the globe. There is some decreasing connectivity in the second period in the spot that, as it is showed in the next section, forms part of the Pacific North American pattern (PNA) in the tropical north Pacific. The Pearson correlation

network has different link density but the structure is quite similar to the intraannual case.

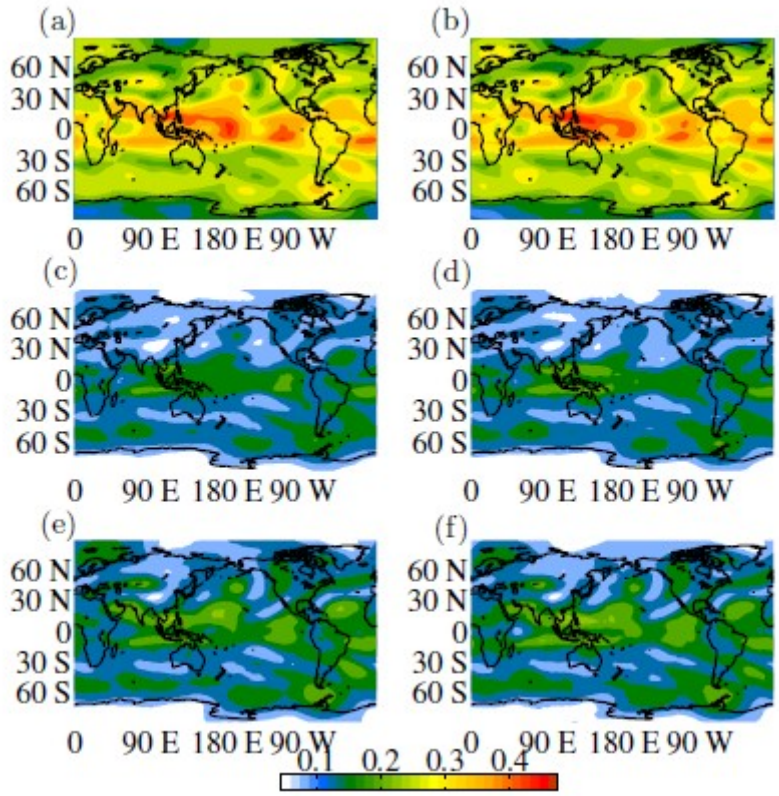

Figure 11 - AWC maps of the ICTP-AGCM internal variability. The networks are built with: PC (1901-1953) (a) and (1954-2006) (b), BP methodology with Δt = 1 (1901-1953) (c), (1954-2006) (d), and BP with Δt = 4 (1901-1953) (e) and (1954-2006) (f).

3.5 Principal component analysis

Considering the influence, or connectivity, of the tropical Pacific, a Principal Component Analysis was done using the NOAA 20th Century Reanalysis data on this region. In particular, the time series within the following coordinates were considered: [90E,110W-30S,30N}. As in the sections above we worked with anomalies of the 200 mb eddy geopotential height and considered the data in halves: [January 1901 - December 1955] and [January 1955 - December 2009].

Figure 12 shows the first two eigenvectors of period (1955-2009), rotated following the simplicity (varimax) criterium. The percentages of explained variance are 14.9 and 9.1, respectively. It is worth mentioning that the leading eigenvector has the same structure than the connectivity degree (Donges et al 2013). Consistently, the first EOF is strongly related with the ENSO pattern.

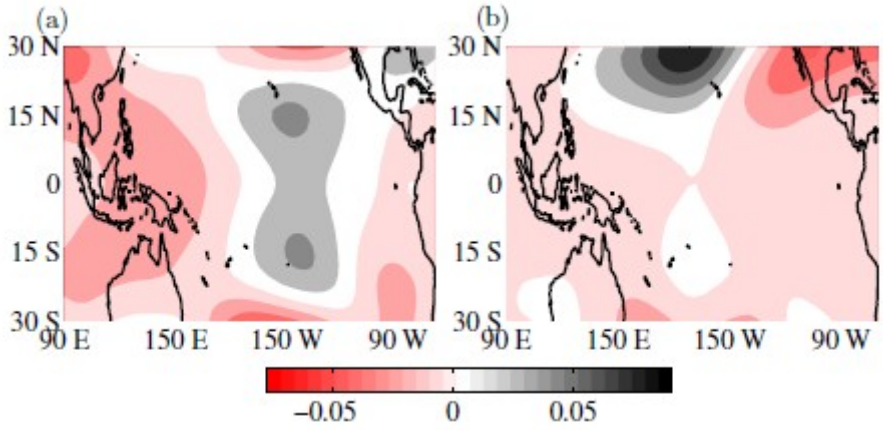

Figure 12 - The first two eigenvectors of the covariance matrix (EOFs) of the NOAA reanalysis data considering the time period (1955-2009) rotated by the simplicity criterium. Variance explained: 14;9% (ENSO pattern related) (a), 9;1% (PNA pattern related) (b).

The maps in Fig. 13 show the regressions of the eddy geopotential height anomalies onto the principal components of the first two EOFs. Clearly, the regression with the leading principal component has a very similar structure than the map of AWC of the ICTP-AGCM forced component, indicating that the ocean forcing is to a large extent from the tropical Pacific. Also, in both periods the second eigenvector is related to the Pacific-North American (PNA) pattern. Note that for the leading EOF in the second period the extropical wave train that propagates from the central Pacific is much stronger than in the first period.

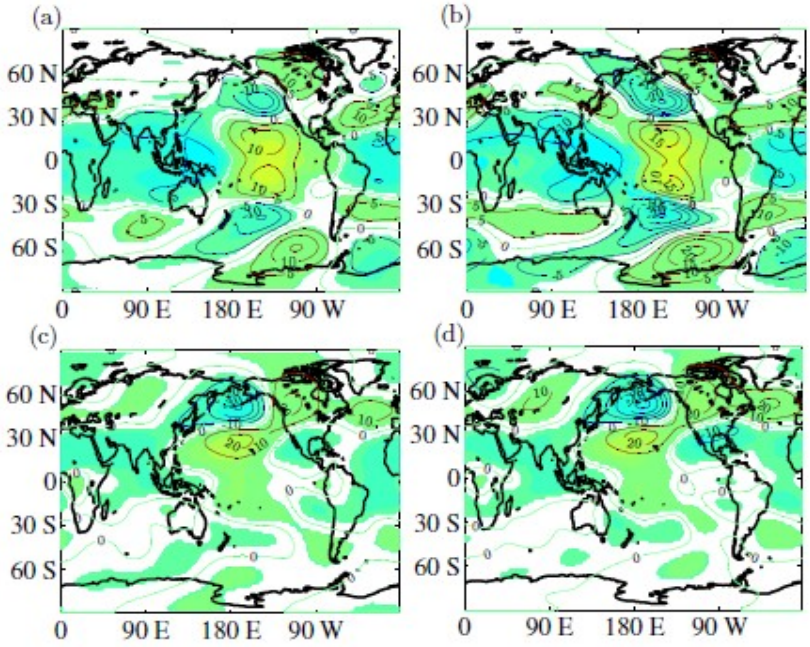

Figure 13 - Regresions of the two principal components obtained with the global eddy geopotential height field where the correlation is statistically significant. (a) and (c) from (1901-1955); (b) and (d) from (1955-2009)

Taking into account that the first two patterns are related to well known modes of variability such as ENSO and PNA, we build the AWC maps for the original data without these principal components (Fig. 14). The AWC function of the Pearson

correlation network without the ENSO related component (Fig. 14a), shows an important decrease mainly in the tropical regions. The overall appearence of the resulting structure is similar to the one obtained for the atmospheric-internal variability of the ICTP-AGCM, showing again the important influence of ENSO in the atmospheric dynamics. On the other hand, panel 14b shows the AWC map of the mutual information with BP symbolic analysis on intraseasonal scale ($\Delta t=1$) without the ENSO related component and the connectivity in the tropical Pacific decreases but to a much lesser extent than in 14a. The general structure in the tropical connectivity is maintained and some subpolar regions become more connected. This suggest that this network connectivity is much lesser ENSO dependent, and thus less influenced by the oceanically-forced component than the Pearson correlation network. In the bottom panels the AWC maps of the mutual information on intraannual scale network (BP with $\Delta t=4$) without the ENSO related component (14c) and without the PNA related component (14d) are shown. In this case it is clear that when one of the principal components is removed, the other related pattern appears more clear. In the north Pacific in the map without ENSO, the dipole pattern that represents the PNA is better defined, while in the other case, when the PNA related component is removed, a center, orthogonal to the PNA dipole, appears.

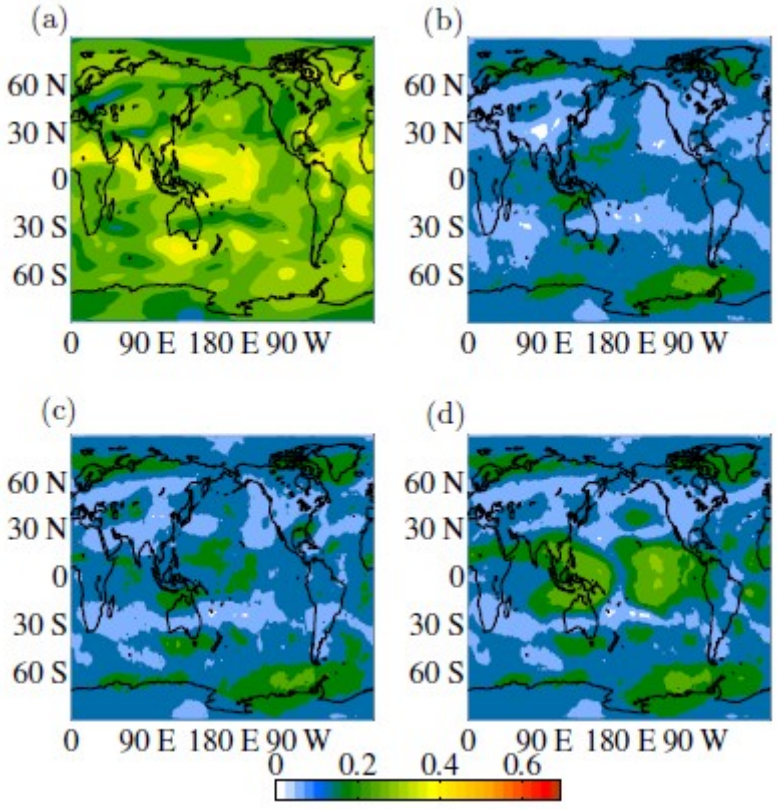

Figure 14 - AWC maps of the NOAA reanalysis using data from the second period (1955-2009). The networks are built after removing one of the two principal components related to ENSO and PNA patterns. PC without ENSO related component (a), MI with intraseasonal time scale without ENSO related component (b), and MI with intraannual time scale without the ENSO and PNA components (c) and (d) respectively.

4 . SUMMARY

We have studied the variability of the 200 mb eddy geopotential height anomaly field by means of networks built using linear and nonlinear statistical similarity measures. The analysis considered two reanalysis data sets (NOAA 20th Cent and NCEP CDAS1) and the output of an Atmospheric General Circulation Model (ICTP-AGCM). This combination allowed to study the evolution of the upper atmosphere connectivity over the 20th century as well as to disentangle the networks due to the forced and internal components. The resulting connectivity structures built using Pearson correlation (linear) or the mutual information (nonlinear) have overall similar spatial features dominated by high connectivity in the tropics and smaller connectivity centers shaped as wave trains in the extratropics.

The use of mutual information calculated with the BP symbolic analysis allows to separate the connectivity depending on the time scale. On intraseasonal scales ($\Delta t=1$), the connectivity of the central and western Pacific show significant changes between both halves of the 20th century: while in the first half the tropical Pacific is fully connected as with the Pearson correlation or mutual information with histograms, in the second period the eastern area appears less connected and the global maximum is on the western Pacific.

On the intraannual time scale ($\Delta t=4$) the main feature is the maximum in connections in the northern Pacific. Finally for the interannual time scale ($\Delta t=12$), the southern subtropical Pacific arises as a connectivity hub, also seen in the AWC constructed with the Pearson correlation and mutual information with histograms but not so clear in the other time scale networks. This fact, together with the evolution of the connectivity of certain regions such as Canada for intraannual networks where the connectivity decreases in the second period while there is an increament in interannual networks, or off the coast of south Brazil that intraseasonal and intraannual networks show more connections in the first half while in PC and MIH networks the opposite behavior is observed, indicates that the BP methodology is useful in separating different time scale processes.

Furthermore, in order to deepen our understanding on the changes in the connectivity during the 20th century, we have studied the AWC time evolution considering a 30-year sliding window of two main boxes located in western (WP) and central Pacific (CP). The temporal evolution in the WP connectivity indicates a decreasing behavior in the beginning of the century until 1940, when it starts increasing until the end for PC, MIH and interannual networks. Intraannual networks, on the other side, present constant connectivity during the first decades and from 1956 onwards a positive trend, while intraseasonal networks increases its connectivity in CP all over the period studied.

In CP the connectivity evolves similarly as in WP for PC, MIH, interannual and intraannual networks. On the other hand the connectivity of intraseasonal networks is very similar to the intraannual networks in this region, decreasing until 1956 and increasing from that moment on. Even though is not trivial to interpretate these results, we might assume that when the connectivity of these main region decreases (increases) in a particular time scale network, the teleconnections that pass through these regions, and are associated with this particular time scale, are weakened (strengthened) in the temporal period considered. In this case, both the mid-century minimum of all the networks connectivity in the central Pacific, as well as the continuous increasing connectivity in the intraseasonal time scales networks in the western Pacific deserve further investigations.

Finally, using the ICTP-AGCM we were able to separate the oceanically-forced component from the atmospheric internal variability and calculate the respective connectivity networks. The results suggest that the main pattern of connectivity captured by the reanalysis networks are due to the oceanically-forced component, particularly on interannual time scales. On intraseasonal time scales the atmospheric internal variability seems to play an important role in determining the network. Construction of the networks after removing the ENSO influence and the PNA pattern allowed to identify their connectivity-related pattern in the network on different time scales. While ENSO pattern seems very important in the Pearson correlation network, in the intraseasonal mutual information network its influence is quite low, especially in the last 60 years. Meanwhile on intraannual time scales the influences of ENSO and PNA patterns are clearly evidenced.

References

Albert R, Barabasi AL (2002) Statistical mechanics of complex networks. Rev Mod Phys 74:47–97. arXiv:cond-mat/0106096

Bandt C, Pompe B (2002) Permutation entropy: A natural complexity measure for time series. Phys Rev Lett 88:174102.

Barabasi AL, Albert R (1999) Emergence of scaling in random networks. Science 286(5439):509–512. arXiv:cond-mat/9910332

Barreiro M, Fedorov A, Pacanowski R, Philander SG (2008) Abrupt Climate Changes: How Freshening of the Northern Atlantic Affects the Thermohaline and Wind-Driven Oceanic Circulations. Annu. Rev. Earth Planet. Sci. 36:33–58.

BarreiroM(2009) Influence of ENSO and the South Atlantic Ocean on climate predictability over Southeastern South America. Clim Dyn DOI 10.1007/s00382-009-0666-9

Barreiro M, Marti AC, Masoller C (2011) Inferring long memory processes in the climate network via ordinal pattern analysis. Chaos 21:013101.

Broennimann S, Stickler A, Griesser T, Fischer AM, Grant A, Ewen T, Zhou T, Scharner M, Rozanov E, Peter T (2009) Variability of large-scale atmospheric circulation indices. Meteorologische Zeitschrift, Vol. 18, No. 4, 379-396.

Compo GP, et al. (2011) The Twentieth Century Reanalysis Project. Quarterly J Roy Meteorol Soc, 137:1-28. DOI: 10.1002/qj.776.

Donges JF, Zou Y, Marwan N, Kurths J (2009) Complex networks in climate dynamics. Eur Phys Lett 87:48007.

Donges JF, Zou Y, Marwan N, Kurths J (2009) The backbone of the climate network. Eur Phys Lett 87:48007.

Donges JF, Petrova I, Loew A, Marwan N, Kurths J (2013) Relationships between eigen and complex network techniques for the statistical analysis of climate data, Preprint: arxiv:1305.6634 [physics.data-an].

Held IM (1983) Stationary and quasi-stationary eddies in the extratropical troposphere: Theory. 127-168. Large scale processes in the atmosphere. Eds. B. J. Hoskins and R. P. Pearce. Academic Press.

James IN (1994) Introduction to circulating atmospheres. Cambridge University Press, Cambridge, UK.

Kalnay E, et al. (1996) The NCEP/NCAR 40-Year Reanalysis Project, Bull Amer Meteorolog Soc 77(3):437-471.

Kucharski F, Molteni F, Bracco A (2006) Decadal interactions between the western tropical Pacific and the North Atlantic Oscillation. Clim Dyn 26: 79-91.

Kucharski F, Bracco A, Yoo JH, Molteni F (2008) Atlantic forced component of the Indian monsoon interannual variability. Geophys Res Lett, 35, L04706, doi:10.1029/2007GL033037.

Kucharski F, Bracco A, Yoo JH, Tompkins A, Feudale L, Ruti P, Dell'Aquila A (2009) A Gill-Matsun-type mechanism explains the Tropical Atlantic influence on African and Indian Monsoon Rainfall. Quart J R Met Soc, 135:569-579. DOI: 10.1002/qj.406

Lintner BR, Chiang JCH (2006) Adjustment of remote tropical climate of El Nino conditions. J Clim 20: 2544-2557.

Martin EA, Paczuski M, Davidsen F (2013) Interpretation of link fluctuations in climate networks during El Ni˜no periods. Eur Phys Lett 102:48003.

Molteni F (2003) Atmospheric simulations using a GCM with simplified physical parametrizations. I. Model climatology and variability in multi-decadal experiments. Clim Dyn 20: 175-191.

Neelin JD, Battisti DS, Hirst AC, Jin FF,Wakata Y, Yamagata T, Zebiak SE (1998) ENSO theory. Journal of Geophysical Research: Oceans (1978–2012) 103 (C7), 14261-14290.

Newman MEJ (2010) Networks: An Introduction. Oxford, Oxford University Press. ISBN 0-19-920665-1.

Palus M, Hartman D, Hlinka J, Vejmelka M (2011) Discerning connectivity from dynamics in climate networks. Nonlin. Processes Geophys., 18, 751-763.

Radebach A, Donner RV, Runge J, Donges JF, Kurths J (2013) Disentangling different types of El Nino episodes by evolving climate network analysis. Phys. Rev. E, 88(5), 052807.

Seager R, Harnik N, Kushnir Y, RobinsonW,Miller J (2003) Mechanisms of hemispherically symmetric climate variability. J Clim Volume 16, Issue 18, p.2960-2978.

Smith TM, Reynolds RW(2004) Improved extended reconstruction of SST (1854–1997). J Clim 17:2466–2477.

Trenberth KE, Branstator GW, Karoly D, Kumar A, Lau N-C, Ropelewski C (1998) Progress during TOGA in understanding and modeling global teleconnections associated with tropical sea surface temperatures. J Geophys Res 103:14291-14324.

Tsonis AA, Roebber PJ (2004) The architecture of climate network. Physica A 333:497-504.

Tsonis AA, Swanson KL, Roebber PJ (2006) What do networks have to do with climate? Bull Amer Meteorol Soc 87:585.

Tsonis AA, Swanson KL (2008) Topology and predictability of El Nino and La Nina networks. Phys Rev Lett 100:228502. doi:10.1103/PhysRevLett.100.228502

Tsonis AA,Wang G, Swanson KL, Rodrigues FA, da Fontura Costa L (2011) Community structure and dynamics in climate networks. Clim Dyn 37:933-940.

Watts DJ, Strogatz SH (1998) Collective dynamics of ’small-world’ networks. Nature 393(6684):440–442. doi:10.1038/30918

Yamasaki K, Gozolchiani A, Havlin S (2008) Climate Networks around the Globe are significantly affected by El Nin˜o. Phys Rev Lett 100:228501.